Multi-Scale Modeling of Calcium Dynamics in Ventricular Myocytes with Realistic Transverse Tubules

Journal:	*Transactions on Biomedical Engineering*
Manuscript ID:	TBME-00542-2011.R1
Manuscript Type:	Special Issue
Date Submitted by the Author:	n/a
Complete List of Authors:	Yu, Zeyun; University of Wisconsin-Milwauke, Computer Science Yao, Guangming; University of Wisconsin-Milwaukee, Computer Science Hoshijima, Masahiko; University of California, San Diego, Medicine Michailova, Anushka; University of California San Diego, Bioengineering Holst, Michael; University of California, San Diego, Mathematics
TIPS:	calcium dynamics, ventricular myocytes, numerical simulation, finite element methods, meshless methods

Multi-Scale Modeling of Calcium Dynamics in Ventricular Myocytes with Realistic Transverse Tubules

Zeyun Yu*, Guangming Yao, Masahiko Hoshijima, Anushka Michailova, and Michael Holst

***Abstract*—Spatial-temporal Ca^{2+} dynamics due to Ca^{2+} release, buffering and re-uptaking plays a central role in studying excitation-contraction (E-C) coupling in both normal and diseased cardiac myocytes. In this paper, we employ two numerical methods, namely, the meshless method and the finite element method, to model such Ca^{2+} behaviors by solving a nonlinear system of reaction-diffusion partial differential equations at two scales. In particular, a sub-cellular model containing several realistic transverse tubules (or t-tubules) is investigated and assumed to reside at different locations relative to the cell membrane. To this end, the Ca^{2+} concentration calculated from the whole-cell modeling is adopted as part of the boundary constraint in the sub-cellular model. The preliminary simulations show that Ca^{2+} concentration changes in ventricular myocytes are mainly influenced by calcium release from t-tubules.**

***Index Terms*—Numerical simulation; finite element methods, meshless methods, calcium dynamics; ventricular myocytes.**

I. Introduction

The high prevalence of heart failure is largely due to our lack of accurate understanding of the complex pathology including abnormal excitation-contraction (E-C) coupling in cardiomyocytes. The architecture of uniquely developed membrane organelles in ventricular myocytes, including transverse tubules (t-tubules) and junctional sarcoplasmic reticulum (jSR), and the arrangement of associated proteins are known to play a major role in dynamically controlling intracellular Ca^{2+} levels, which in turn regulate cardiac contraction and other cellular functions [1]. For its central role in E-C coupling, modeling Ca^{2+} release and concentration change has been an active research area and is typically studied in two ways: stochastic approaches that employ Monte Carlo simulation [2] and deterministic approaches based on partial differential equations (PDEs) [3]. While stochastic simulation at the nanometer scale provides elementary information on Ca^{2+} dynamics, cardiac cell contraction is most closely related to the intracellular Ca^{2+} concentration level $[Ca^{2+}]_i$ [4]. For this reason, our interest in the present paper is to investigate spatial-temporal variations of intracellular Ca^{2+} concentration at cellular and subcellular levels, where the stochastic behavior of Ca^{2+} dynamics is so insignificant that deterministic methods utilizing PDEs are more appropriate.

Z. Yu and G. Yao are with Department of Computer Science at University of Wisconsin-Milwaukee, WI 53211.

M. Hoshijima, A. Michailova and M. Holst are with Department of Medicine, Department of Bioengineering, and Department of Mathematics and Physics, respectively, at University of California-San Diego, CA 92093.

*Corresponding author (phone: 414-229-2960; email: yuz@uwm.edu).

Most of the previous work using PDEs to study Ca^{2+} dynamics was conducted based on idealized geometries such as cylindrical shapes [3], [5]. As pointed out in [2], [3], geometric changes may significantly influence the behaviors of Ca^{2+} dynamics both locally and globally. For example, the heart failure is closely related to rearrangement or lack of t-tubules in cardiac cells [6], [7]. In fact, a recent study by Cheng et al. [8], which utilizes a single t-tubular branch generated from light microscopic images, suggests that the quantitative understanding of Ca^{2+} signaling requires more accurate knowledge of t-tubular ultra-structures. Thus, one of the focuses in the present paper is to include nanometer-scale, realistic surface geometries of multiple t-tubules that are constructed from three-dimensional (3D) electron microscopic (EM) images of the ventricular myocytes of an adult mouse [9]. It is worth noting that in mice both transverse tubules and axial tubules are found and often known as transverse-axial tubules (or TATs) [10]. However, t-tubular branches are naturally more frequently observed than axial tubules. In addition, the 3D EM tomographic data we have used for the current study is so thin that there is no obvious axial tubule in the image. Therefore, we shall still adopt the name "t-tubule" instead of "TAT" throughout the present paper.

The underlying PDEs describing Ca^{2+} dynamics in ventricular myocytes may be numerically solved by such techniques as the finite difference method (FDM) [11], the finite element method (FEM) [12], [13], the finite volume method (FVM) [14], and the boundary element method (BEM) [15]. All these methods are mesh-based, meaning that meshes or grids must be constructed on the problem domain. Another numerical approach known as meshless method [16] does not require explicit meshes and thus has gradually become popular in the past two decades. Our recent work (unpublished) has shown that this method can be easily adapted to handle very large systems. However, numerically it is not as stable as the finite element method. For these reasons, in the current study we employ both meshless and finite element methods to study Ca^{2+} dynamics at different scales.

II. Geometric and Mathematical Modeling

A. The Geometric Model

Fig. 1(a) shows the geometric model containing several t-tubules extracted from the ventricular myocytes of an adult mouse. The details of electron microscopic imaging and 3D tomographic reconstruction can be found in [9]. The algorithmic

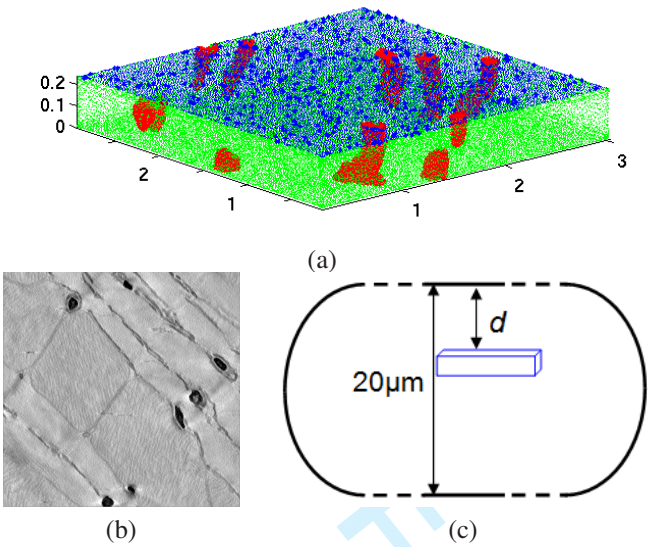

Fig. 1. (a) Multiple t-tubule geometry and its surrounding box domain, denoted by Ω. The red color in Ω represents t-tubules (denoted by Γ_1), the top blue face of the box (denoted by Γ_2) satisfies the Dirichlet boundary condition, and a reflective boundary condition is assumed on the remaining boundary faces (in green). (b) One slice of the 3D electron tomographic map, showing t-tubules in dark regions surrounded by jSR. (c) The model in (a) is placed at various locations in a simplified whole-cell model at a distance d ($d = 8\mu m$, $2\mu m$, or $0\mu m$) from the cell membrane.

details of image processing and boundary segmentation are described in [17]. Fig. 1(b) shows one slice of the reconstructed tomographic map, where dark regions are t-tubules surrounded by jSR (not considered in this study). The rectangle-shaped model in Fig. 1(a), denoted by $\Omega \subset \mathbb{R}^3$, is the problem domain in our simulations and the dimension of the box is measured as $2.81\mu m \times 2.79\mu m \times 0.24\mu m$. The boundary Γ_1 (in red) represents realistic t-tubules and Γ_2 (in blue) is the top face of Ω. Because the location of the constructed t-tubules in the ventricular myocyte is unknown and we are also interested in the roles of t-tubules and cell membrane in calcium dynamics, we shall consider three cases in our simulations by placing the model in Fig. 1(a) in a simplified whole-cell model such that the top face Γ_2 is at a distance d ($d = 8\mu m$, $2\mu m$, or $0\mu m$) away from the cell membrane (see Fig. 1(c)).

B. Governing Equations

The following nonlinear reaction-diffusion equations, defined on the model described above, are modified from [18]:

$$\begin{aligned}
&\frac{\partial [Ca^{2+}]_i}{\partial t} = D_{Ca}\nabla^2[Ca^{2+}]_i - \sum_{m=1}^{3} R_{Bm} - R_{Bs}, && \Omega,\\
&\frac{\partial [CaB_m]}{\partial t} = D_{CaBm}\nabla^2[CaB_m] + R_{Bm}, \quad m = 1,2,3, && \Omega,\\
&\frac{\partial [CaB_s]}{\partial t} = R_{B_s}, && \Omega,\\
&\frac{\partial [Ca^{2+}]_i}{\partial t} = D_{Ca}\nabla^2[Ca^{2+}]_i + J_{Caflux}, && \Gamma_1,\\
&[Ca^{2+}]_i = [Ca^{2+}]_{i_0}, && \Gamma_2,
\end{aligned} \tag{1}$$

with the following initial conditions:

$$\begin{aligned}
&[Ca^{2+}]_i = 0.10\mu M, \quad [CaB_1] = 11.92\mu M,\\
&[CaB_2] = 0.97\mu M, \quad [CaB_3] = 0.13\mu M,\\
&[CaB_s] = 6.36\mu M.
\end{aligned}$$

The boundary Γ_2 (the top face in Fig. 1(a)) satisfies the Dirichlet boundary condition, and a reflective boundary condition is assumed on the remaining faces of the box. The Ca^{2+} concentration, $[Ca^{2+}]_{i_0}$, on Γ_2 is obtained from the whole-cell modeling using the messless method (see below).

In our model, three types of mobile Ca^{2+} buffers (Fluo-3, ATP, and calmodulin, denoted by B_m, $m = 1, 2, 3$, respectively), and one type of stationary Ca^{2+} buffers (troponin, denoted by B_s) are considered. Their concentrations are denoted by $[Ca^{2+}]_i$, $[CaB_m], m = 1, 2, 3$, $[CaB_s]$, respectively. The reactions between Ca^{2+} ions and buffers are defined as:

$$R_{Bm} = k_+^m \left([B_m] - [CaB_m]\right)[Ca^{2+}]_i - k_-^m [CaB_m], \tag{2}$$

$$R_{Bs} = k_+^m \left([B_s] - [CaB_s]\right)[Ca^{2+}]_i - k_-^m [CaB_s], \tag{3}$$

where $m = 1, 2, 3$.

At the resting (initial) state, we assume uniform distributions of all the buffers throughout the cytosol. The resting concentrations of mobile and stationary buffers satisfy equilibrium conditions (i.e., $R_{Bm} = R_{Bs} = 0$) [19] with the resting Ca^{2+} concentration at $0.1\mu M$. The total Ca^{2+} flux, J_{Caflux}, on the t-tubule surface is defined as in [18]:

$$J_{Caflux} = J_{Ca} + J_{NCX} - J_{pCa} + J_{Cab}, \tag{4}$$

where calcium influx/efflux through L-type calcium channels (LCCs, J_{Ca}), sodium-calcium exchangers (NCXs, J_{NCX}), calcium pump efflux (J_{pCa}), and calcium background leak influx (J_{Cab}) are included. The current densities, I_{Ca}, I_{NCX}, I_{pCa}, and I_{Cab}, are calculated the same as in [18]. The physical constants and parameters are taken from [18], [20]. To calculate the total Ca^{2+} flux, J_{Caflux}, each of the current densities is converted into Ca^{2+} flux by using:

$$J_i = \beta_i \frac{V_{mc}}{S_{mc}} \left(\frac{1}{2F}\frac{C_m}{V_{cell}}\right) I_i, \tag{5}$$

with $i = Ca, NCX, pCa$, or Cab. The capacitance to rendered volume ratio (C_m/V_{cell}) is assumed to be $8.8pF/pL$ [21]. Note that S_{mc} is the total area of t-tubule membrane where Ca^{2+}-related channels reside and V_{mc} is the volume of the model. In Fig. 1(a), $V_{mc} = 1.782\mu m^3$, and $S_{mc} = 0.919\mu m^2$. The model-dependent scaling parameter, $\beta_{Ca} = 4.0$, and $\beta_{NCX} = \beta_{pCa} = \beta_{Cab} = 1.0$. The voltage clamp protocol is assumed to hold the potential $-50mV$ with an electric pulse of $10mV$ for $70ms$ [18].

III. Methodology

To solve the system of equations in (1), we use an explicit time-stepping method in time and the finite element method in space. Since we consider Γ_2 at different locations in a simplified ventricular myocyte, predicting the initial Ca^{2+} concentration, $[Ca^{2+}]_{i_0}$, on Γ_2 is necessary and is performed by using the meshless method.

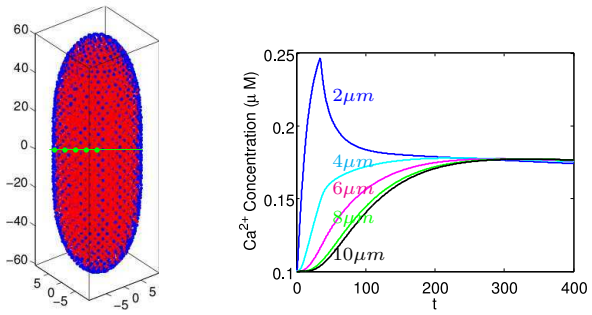

(a) (b)

Fig. 2. (a) the whole-cell model of approximately $120\mu m \times 20\mu m \times 20\mu m$, with t-tubules and all intra-cellular structures excluded. Indicated in green is a scanning line going through the center of the cell, with five feature spots that are $2\mu m$, $4\mu m$, $6\mu m$, $8\mu m$, and $10\mu m$ away from the cell membrane. (b) local Ca^{2+} transients taken at the five feature spots shown in (a).

A. The Meshless Method

A simplified whole-cell model, as shown in Fig. 2(a), is considered. To predict spatial-temporal Ca^{2+} concentrations in a large domain, the meshless method is a good choice compared with other numerical methods, for its implementation simplicity, time efficiency, and effectiveness in dealing with complicated geometries [22]. In particular, the finite difference method has been utilized in [5] for whole-cell calcium modeling, but the meshless method can handle smooth yet complex domain boundaries more effectively. In our meshless method, the operator-splitting method is used to decouple the PDEs and to separate nonlinear sources and the Laplacian operators. The local radial basis function collocation method (LRBFCM) [16] is employed to approximate Laplacian terms at every time-step. With the predicted spatial-temporal Ca^{2+} concentrations, Fig. 2(b) shows local Ca^{2+} transients at five representative spots that are $2\mu m$, $4\mu m$, $6\mu m$, $8\mu m$, and $10\mu m$ away from the cell membrane. For the sub-cellular modeling problem (Fig. 1(a)), we consider three locations (Fig. 1(c)), where $d = 0\mu m, 2\mu m, 8\mu m$. The concentrations at these locations in the whole-cell modeling shall be used below as the boundary condition for Γ_2 in the system (1).

B. The Finite Element Method

With the initial concentration $[Ca^{2+}]_{i0}$ predicted on Γ_2, we employ the finite element toolkit FETK (http://FETK.org) and the CSMOL software (http://mccammon.ucsd.edu/smol/) [23] to solve the system (1) on the geometric model shown in Fig. 1(a). The software toolkit called GAMer [24] is used to discretize the complex domain into a tetrahedral mesh. In the present simulation, we have $83,614$ nodes (vertices) and $350,249$ tetrahedra. The time-step size is chosen as $4ms$. It takes about 55 minutes to compute the concentrations for a time period of $[0, 400ms]$ on a single Intel Xeon-based processor (3.00GHz). The numerical results below are visualized by Meshlab and MATLAB 2.7.7.

IV. Results

In our current study, the SR has been excluded from the finite element simulations shown below. Fig. 3 shows the results with the presence of $100\mu M$ Fluo-3, where the geometric model used is given in Fig. 1(a). The global and local Ca^{2+} transients reach the peaks at about $72ms$ when the LCC current is completely blocked. Fig. 3 (a)–(b) show the voltage-clamp protocol and the whole-cell L-type Ca^{2+} current as used in [18].

In Fig. 3 (c)–(l), we show three boundary conditions on Γ_2, where Γ_2 is assumed to be $8\mu m$ (blue lines), $2\mu m$ (green lines), and $0\mu m$ (red lines) away from the cell membrane (see Fig. 1(c)). Fig. 3 (c)–(e) show the averaged current densities of Na^+/Ca^{2+}exchangers, Ca^{2+} pumps and Ca^{2+} leaks, assuming a uniform distribution of Ca^{2+} inside the model. Fig. 3(f) shows the averaged Ca^{2+} concentration over time. The time-varying concentrations of the calcium-bound mobile and stationary buffers are shown in (g)–(j) in Fig. 3. In the presence of LCC current densities, these concentrations rapidly increase. After the LCC current is blocked, the concentrations of the calcium-bound buffers gradually decrease and become stable when the free Ca^{2+} concentration is stable. In all these results, the curves are almost identical in the two conditions where Γ_2 is $8\mu m$ and $2\mu m$ away from the cell membrane, suggesting that the main contribution to calcium concentration changes in ventricular myocytes comes from t-tubules except in the regions near the cell membrane.

While the averaged Ca^{2+} concentration within the cytosol of the model is shown in Fig. 3(f), we also consider two feature spots along a scanning line going vertically through the center of the box in Fig. 1(a). These two spots are $0.235\mu m$ and $0.0038\mu m$ away from the top surface Γ_2 of the box, and the calcium concentration changes over time are given in Fig. 3 (k)&(l), respectively. Again, when the model is placed near the cell membrane, we observe significantly higher Ca^{2+} concentration than the other two cases. When the feature spot is chosen near the top surface Γ_2, the other two cases (green and blue lines in Fig. 3(l)) are also distinguishable.

The model is able to predicate local Ca^{2+} transient peaks at approximately $72ms$. Fig. 4 and Fig. 5 show the 3D local Ca^{2+} transients when $t = 72ms$. The local Ca^{2+} transients near the t-tubular surface are about $10 \sim 20\%$ higher than elsewhere. When the distance from the cell membrane to Γ_2 increases (i.e., going from $0\mu m$, $2\mu m$ to $8\mu m$), the Ca^{2+} concentration undergoes a quick ($\sim 15\%$) decrease and then becomes stable, as also seen in [8], suggesting that the influence from the surface membrane rapidly diminishes. The difference between the bulk and subsarcolemmal Ca^{2+} concentrations had been discussed in previous studies (i.e., [25]). Another factor of the Ca^{2+} concentration changes observed in Fig. 4 and Fig. 5 might be due to the lack of calcium release from SR in our current study.

V. Conclusion

In this paper we employed the finite element method and realistic EM structures of t-tubules to investigate calcium dynamics involving calcium releasing, buffering, and re-uptaking at the sub-cellular scale. Different boundary conditions are imposed on the sub-cellular model by placing the model at three different locations relative to the cell membrane of

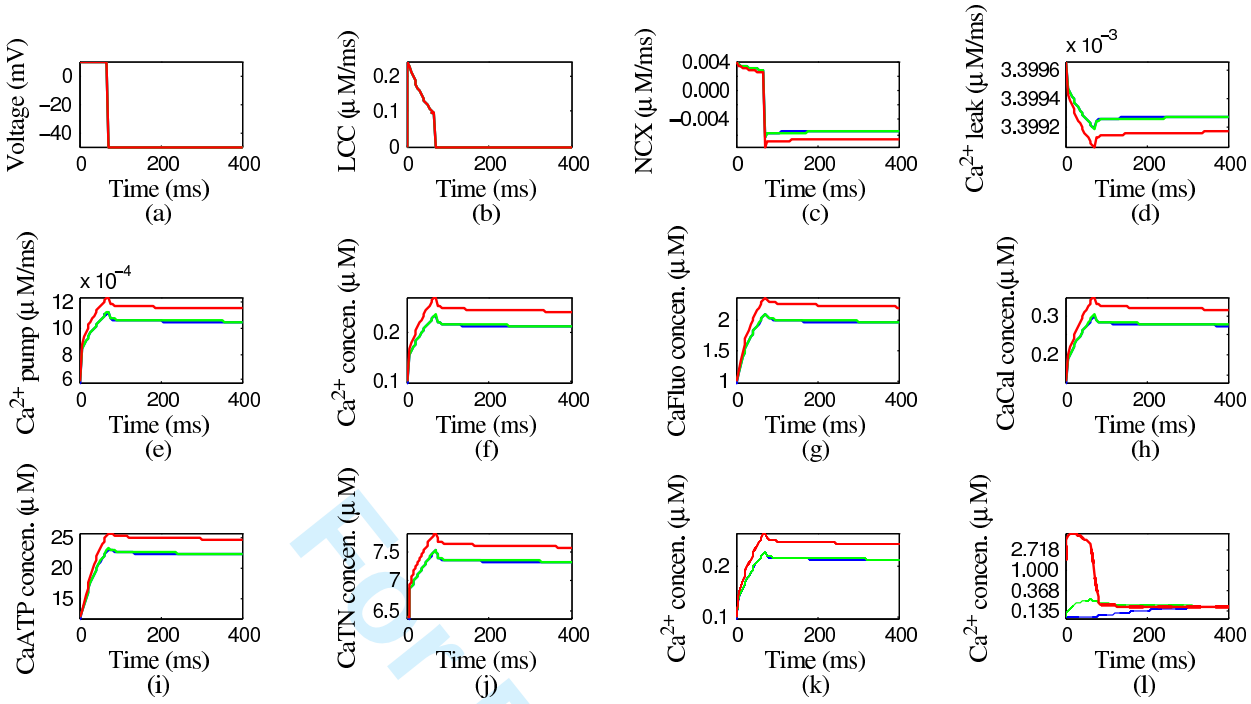

Fig. 3. Calcium signaling simulations with realistic t-tubule membrane. The upper boundary Γ_2 of the sub-cellular model (Fig. 1(a)) is assumed to be $8\mu m$ (blue lines), $2\mu m$ (green lines), and $0\mu m$ (red lines) away from the cell membrane (also see Fig. 1). Note that in most of the simulations plotted here, the blue lines are almost identical to the green lines. (a)-(b) The voltage-clamp protocol and the whole-cell LCC current used in the simulation. (c)-(f) Predicted global Na^+/Ca^{2+}, Ca^{2+} pump and leak currents and global average Ca^{2+} transient when Ca^{2+} is uniformly distributed inside the cell. (g)-(j) Predicted average concentrations of calcium-bound mobile and stationary buffers. (k)-(l) Local Ca^{2+} transients taken at two feature spots that are $0.235\mu m$ (k) and $0.0038\mu m$ (l) away from Γ_2.

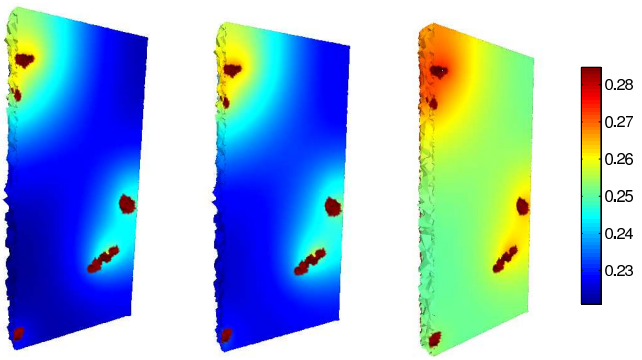

Fig. 4. 3D views of the Ca^{2+} concentrations at the $[Ca^{2+}]_i$ peak of $72ms$ when the sub-cellular model in Fig. 1(a) is placed $8\mu m$ (left), $2\mu m$ (middle), and $0\mu m$ (right) away from the cell membrane. Note that the left portion (about one half) of the domain has been cut out.

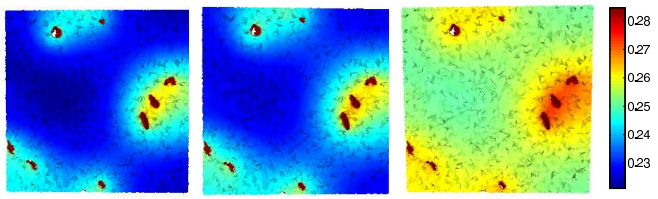

Fig. 5. Cross-section views of the Ca^{2+} concentrations at the $[Ca^{2+}]_i$ peak of $72ms$ when the sub-cellular model in Fig. 1(a) is placed $8\mu m$ (left), $2\mu m$ (middle), and $0\mu m$ (right) away from the cell membrane. About a half of the domain has been cut out in the front to show the cross-section views.

a simplified ventricular myocyte. The boundary values are borrowed from the whole-cell simulations pre-computed by using the meshless method. The preliminary results show that t-tubules, as compared to the cell surface membrane, play a major role in regulating Ca^{2+} concentration changes in ventricular myocytes.

References

[1] D. M. Bers, "Calcium cycling and signaling in cardiac myocytes," *Annual Reviews Physiology*, vol. 70, pp. 23–49, 2008.

[2] X. Koh, B. Srinivasan, H. S. Ching, and A. Levchenko, "A 3D monte carlo analysis of the role of dyadic space geometry in spark generation," *Biophys. J.*, vol. 90, pp. 1999–2014, 2006.

[3] L. T. Izu, S. A. Means, J. N. Shadid, Y. Chen-Izu, and C. W. Balke, "Interplay of ryanodine receptor distribution and calcium dynamics," *Biophys. J.*, vol. 91, pp. 95–112, 2006.

[4] D. M. Bers, "Cardiac excitation-contraction coupling," *Nature*, vol. 415(10), pp. 198–205, 2002.

[5] A. Michailova, F. DelPrincipe, M. Egger, E. Niggli, "Spatiotemporal features of Ca2+ buffering and diffusion in atrial cardiac myocytes with inhibited sarcoplasmic reticulum," *Biophysical Journal*, vol. 83, pp. 3134–3151, 2002.

[6] F. Brette, C. Orchard, "T-tubule function in mammalian cardiac myocytes," *Circulation Research*, vol. 92, pp. 1182–1192, 2003.

[7] C. Orchard, M. Pasek, and F. Brette, "The role of mammalian cardiac t-tubules in excitation-contraction coupling: experimental and computational approaches," *Exp Physiol*, vol. 94, pp. 509–519, 2009.

[8] Y. Cheng, Z. Yu, M. Hoshijima, M. Holst, A. McCulloch, J.A. McCammon and A.P. Michailova, "Numerical analysis of ca^{2+} signaling in rat ventricular myocytes with realistic transverse-axial tubular geometry and inhibited sarcoplasmic reticulum," *PLoS Comput Biol*, vol. 6(10), e1000972, 2010.

[9] T. Hayashi, M.E. Martone, Z. Yu, A. Thor, M. Doi, M. Holst, M.H. Ellisman, and M. Hoshijima, "Three-dimensional reconstruction reveals new details of membrane systems for calcium signaling in the heart,"

Journal of Cell Science, vol. 122, pp. 1005–1013, 2009.

[10] M.S. Forbes, L.A. Hawkey, and N. Sperelakis, "The transverse-axial tubular system (TATS) of mouse myocardium: its morphology in the developing and adult animal," *Am J Anat.*, vol. 170, no. 2, pp. 143-162, 1984.

[11] L. Wu and Y. Kwok, "A front-fixing finite difference method for the evaluation of american options," *Comput. Math. Applic.*, vol. 6, pp. 83–83, 1997.

[12] D. Braess, *Finite Elements. Theory, Fast Solvers and Applications in Solid Mechanics*. Cambridge University Press, 2001.

[13] J. Melenk and I. Babuska, "The partition of unity finite element method: Basic theory and applications," *Comput. Meths. Appl. Mech. Engrg.*, vol. 139, pp. 289–314, 1996.

[14] R. Eymard, T. Gallouet, and R. Herbin, "Finite volume methods," in *Techniques of Scientific Computing, Part III, Handbook of Numerical Analysis, VII*, P. G. Ciarlet and J. L. Lions, Eds. North-Holland, Amsterdam, 2000, pp. 713–1020.

[15] R. Schaback, "Convergence analysis of methods for solving general equations," in *Boundary Elements XXVII*, A. Kassab, C. Brebbia, E. Divo, and D. Poljak, Eds. WITPress, Southampton, 2005, pp. 17–24.

[16] B. Šarler and R. Vertnik, "Meshfree explicit local radial basis function collocation method for diffusion problems," *Computers and Mathematics with Applications*, vol. 51, pp. 1269–1282, 2006.

[17] Z. Yu, M. Holst, T. Hayashi, C.L. Bajaj, M.H. Ellisman, J.A. McCammon, and M. Hoshijima, "Three-dimensional geometric modeling of membrane-bound organelles in ventricular myocytes," *Journal of Structural Biology*, vol. 164, no. 3, pp. 304-313, 2008.

[18] S. Lu, A. Michailova, J. Saucerman, Y. Cheng, Z. Yu, T. Kaiser, W. Li, R. Bank, M. Holst, J. Mccammon, T. Hayashi, M. Hoshijima, P. Arzberger, and A. McCulloch, "Multiscale modeling in rodent ventricular myocytes," *Engineering in Medicine and Biology Magazine, IEEE*, vol. 28, no. 2, pp. 46–57, mar. 2009.

[19] V. Matveev, R. S. Zucker, and A. Sherman, "Facilitation through buffer saturation: Constraints on endogenous buffering properties," *Biophysical Journal*, vol. 86(5), pp. 2691–2709, 2003.

[20] R. Hinch, J. Greenstein, A. Tanskanen, L. Xu, and R. Winslow, "A simplified local control model of calcium-induced calcium release in cardiac ventricular myocytes," *Biophysical Journal*, vol. 87, no. 6, pp. 3723 – 3736, 2004.

[21] H. Satoh, L. Delbridge, L. Blatter, and D. Bers, "Surface:volume relationship in cardiac myocytes studied with confocal microscopy and membrane capacitance measurements: species-dependence and developmental effects," *Biophys J.*, vol. 70(3), pp. 1494–1504, 1996.

[22] A. Karageorghis, C. S. Chen, and Y.-S. Smyrlis, "Matrix decomposition rbf algorithm for solving 3D elliptic problems," *Engineering Analysis with Boundary Elements*, vol. 33, pp. 1368–1373, 2009.

[23] Y. H. Cheng, J. K. Suen, D. Q. Zhang, S. D. Bond, Y. J. Zhang, Y. H. Song, N. A. Baker, C. L. Bajaj, M. J. Holst, and J. A. McCammon, "Finiteelement analysis of the time-dependent smoluchowski equation for acetylcholinesterase reaction rate calculations," *Biophys. J.*, vol. 92, pp. 3397–3406, 2007.

[24] Z. Yu, M. Holst, and J.A. McCammon, "High-fidelity geometric modelling for biomedical applications," *Finite Elements in Analysis and Design*, vol. 44, pp. 715–723, 2008.

[25] A.W. Trafford, M.E. Diaz, S.C. O'Neill, and D.A. Eisner, "Comparison of subsarcolemmal and bulk calcium concentration during spontaneous calcium release in rat ventricular myocytes," *J Physiol.*, vol. 488, pp. 577–586, 1995.

Zeyun Yu received his Ph.D. degree from The University of Texas-Austin in 2006. He was a postdoctoral scholar at UCSD before he joined The University of Wisconsin-Milwaukee in 2008 as an assistant professor in computer science. His research focuses on image analysis, geometric processing and visualization, and scientific computing in biomedicine.

Guangming Yao received her Ph.D. degree in computational mathematics from The University of Southern Mississippi in 2010. She is currently a post-doctoral associate in Department of Computer Science at The University of Wisconsin at Milwaukee. Her research interest includes numerical analysis of partial differential equations, computational biology, finite element methods, meshless methods, and optimization theory and applications.

Masahiko Hoshijima is an associate adjunct professor of medicine and a member of Center for Research in Biological Systems at UCSD. His lab studies the structural and functional remodeling of membrane and cytoskeletal micro-domains in various cardiac disease by integrating transgenic mouse technologies, in vivo physiology, cell and molecular biology, and advanced microscopic imaging technologies including EM tomography. He has a M.D. and a Ph.D. in Biochemistry from Kobe University School of Medicine.

Anushka Michailova is associated project scientist in the Bioengineering Department at UCSD. She is Co-PI of the NBCR core project: Multiscale Modeling of Biomedical Systems under Normal and Pathological Conditions. Dr. Michailovas research focuses on using mathematical methods to model and better understand cardiac cells, delineating Ca2+ mediated signaling, excitation-contraction coupling, and energy metabolism. She has Masters degree in Physics and Ph.D. in Molecular Biology and Genetics from the Sofia University in 1996.

Michael Holst received his Ph.D. degree from the University of Illinois at Urbana-Champaign in 1993. He is a professor of mathematics and co-director of both the Center for Computational Mathematics and the Computational Science, Mathematics, and Engineering Doctoral Program at UCSD. He is also a senior scientist at the Center for Theoretical Biological Physics (CTBP) and a core investigator at the NBCR.